

Attenuation of the Multiple Reflection-Refraction in 2-D Common-Shot Gather via Random-Derangement-Based FX Cadzow Filter

Yanglijiang Hu, Dawei Liu, Xiaokai Wang[✉], *Member, IEEE*, Zhonghua Zhao, and Wenchao Chen[✉]

Abstract—The attenuation of coherent noise plays a crucial role in reflection seismology but still poses some technical challenges. The multiple reflection–refraction (MRR) is one of the main coherent noises in land seismic surveys. The Cadzow filter can effectively attenuate incoherent noise. But it struggles in attenuating coherent noise. After keeping reflection events relatively horizontal, some researchers randomly rearrange the trace orders of the input data to realign coherent noise in an incoherent position so that the Cadzow filter can treat the realigned coherent noise as incoherent noise. Accordingly, a random-derangement-based FX Cadzow filter is proposed to attenuate MRRs in 2-D common-shot gathers based on the linear feature of MRR events and randomization of limited trace orders of the input data. In practice, after linear-move-out (LMO) with an estimated dip, the input data are divided into several small windows to obtain a group of relatively horizontal MRR events. Then, these windows are randomized and filtered one by one. Due to the limited trace orders of each window, there are many possible rearrangements after randomization. Some rearrangements may lead to undesirable filtering performance. To obtain the rearrangements that lead to good filtering performance, each window’s trace orders are randomly deranged by resampling from the input orders with uniform distribution. A 2-D synthetic data experiment shows the influence of different rearrangements on the filtering performance. Both 2-D synthetic data and 2-D field data demonstrate that the proposed method outperforms the 2-D FK filter to attenuate both aliased and nonaliased MRRs.

Index Terms—2-D common-shot gather, FX Cadzow filter, multiple reflection–refraction (MRR), random operator.

I. INTRODUCTION

THE attenuation of coherent noise plays a key role in reflection seismic exploration because a high signal-to-noise ratio (SNR) is a prerequisite for many seismic data

Manuscript received September 11, 2020; revised November 23, 2020 and December 26, 2020; accepted January 10, 2021. This work was supported in part by the National Key Research and Development Plan under Grant 2017YFB0202902, in part by the National Natural Science Foundation of China under Grant 41774135 and Grant 41974131, and in part by the Exploration and Development Research Institute of Daqing Oilfield Company. (Corresponding author: Wenchao Chen.)

Yanglijiang Hu, Dawei Liu, Xiaokai Wang, and Wenchao Chen are with Xi’an Jiaotong University, Xi’an 710049, China (e-mail: hylj2018@stu.xjtu.edu.cn; liudawei2015@stu.xjtu.edu.cn; xkwang@xjtu.edu.cn; 15156981@qq.com).

Zhonghua Zhao is with the Exploration and Development Research Institute of Daqing Oilfield, Daqing 163453, China (e-mail: zhaozhonghua@petrochina.com.cn).

Color versions of one or more figures in this letter are available at <https://doi.org/10.1109/LGRS.2021.3051620>.

Digital Object Identifier 10.1109/LGRS.2021.3051620

procedures such as amplitude versus offset analysis [1]. Various methods have been proposed to attenuate coherent noise based on the differences in specific properties between reflections and target coherent noise [2], [3]. However, the suppression of coherent noise, such as multiples [4] and ground roll [5], still poses some technical challenges.

In land seismic surveys with strong reflective interfaces under the free surface (e.g., as ground), the multiple reflection–refraction (MRR) is one of the main coherent noises that seriously affects the SNR of seismic records. A strong reflective interface exists between two strata with a significant velocity difference. When the low-velocity layer overlies the high-velocity layer, refraction is formed by a seismic wave passing through the low-velocity overlying layer and reaching the strong reflective interface at a critical angle. The second refraction occurs when it travels to the free surface and gets reflected in the interface at the same critical angle. By analogy, when this process continues, a group of multiple reflections and secondary refractions are formed. Such a formation is called an MRR. It is characterized by a group of parallel oblique events with a constant apparent dip [6]. This dip depends on the velocity of the high-velocity layer. When multiple strong reflective interfaces with deeper high-velocity layers exist, multiple groups of MRRs with different apparent dips are generated. This phenomenon is illustrated by a 2-D common-shot gather obtained by bilateral acquisition in east China, as shown in Fig. 1. MRRs appear as three main groups of parallel oblique events, such as those marked by the blue, yellow, and red lines in Fig. 1, respectively. In addition, MRR events are continuous and cause significant damage to the reflections. The reflection events are nearly invisible, especially around the near-shot traces denoted by a red arrow, where MRRs’ energy focuses on.

There are many traditional methods based on the FK transform [7], Radon transform [8], [9], curvelet transform [10], wavelet transform [11], and so on to suppress this surface-related linear coherent noise. However, because they separate the reflection and coherent noise based on the difference in apparent velocity, they may damage the reflection when suppressing coherent noise with similar apparent velocities. Meanwhile, the filters based on singular value decomposition (SVD) have been used to attenuate noise in seismic data [12], [13]. They were first applied by Freire and Ulrych [14] in the time–space domain to separate the up-going and down-going

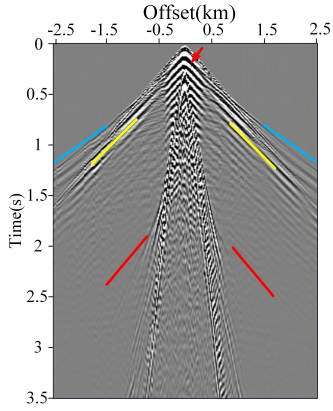


Fig. 1. 2-D common-shot gather.

waves of the vertical seismic profile. The SVD-based filters in the time–space domain have been proven to attenuate the ground roll [5], [15]. However, they may obtain suboptimal results for the reflection dipping events [16]. Better performance for recovering the reflection events with limited different dips is obtained by extending the SVD-based filters to the frequency domain. One commonly used version is the Cadzow filter [17], [18], which can be easily extended to multiple dimensions beyond 2-D. The filters based on singular spectrum analysis (SSA) [19] and multichannel SSA (MSSA) [20] are equivalent to the Cadzow filter. They enhance the reflection by reforming constant-frequency slices into Hankel matrices [21] and outperform the SVD-based filter in the time–space domain by suppressing both coherent [22] and incoherent noises [23]. Their denoising performance depends on the difference between reflection and noise coherence. Coherent noise also has high coherence with reflection. Thus, they have an undesirable performance in suppressing coherent noise. To suppress coherent noise, a general random operator [24] is proposed to destroy the coherence of coherent waves by randomly rearranging the trace orders of the input data while not affect the waves appearing as relatively horizontal events. After flattening reflection events and destroying coherent noise coherence with the general random operator, it is easier for the MSSA-based filters to distinguish coherent noise and reflections. This method has been used to attenuate coherent and incoherent noises in cross-spread gathers simultaneously or in the common-depth-point gathers [25] and interpolate [26].

Inspired by the general random operator’s usages, a random-derangement-based FX Cadzow filter is proposed to attenuate MRRs in 2-D common-shot gathers based on the linear feature of MRR events and randomization of limited trace orders of the input data. Due to the parallelism within each group of linear MRR events, a group of MRR events are easier to be flattened than reflection events. In the first, a group of MRR events in the input data are flattened by applying linear-move-out (LMO) correction [27] with an estimated dip. Consider the spatial variations during the seismic wave propagation, the data after LMO are divided into several small overlapping windows for randomizing and filtering. Due to the limited trace orders of each window, there are many possible rearrangements after a general random operator [28]. Some rearrangements may lead to undesirable filtering performance. To obtain the

rearrangements that lead to good filtering performance, a random derangement operator that randomly deranges the trace orders of window is proposed. It is based on a rejection method that quickly generates a new permutation by resampling from the input orders with uniform distribution. The significant influence of different rearrangements on filtering performance is shown by a 2-D synthetic data experiment. First, the FX Cadzow filter is reviewed. Second, our method is depicted. Finally, the application on 2-D synthetic data and a 2-D common-shot gather demonstrates the effectiveness of our method in attenuating MRRs compared with a 2-D FK filter.

II. THEORY

A. FX Cadzow Filter

The FX Cadzow filtering [21] is a rank-reduction procedure. For the input data consisting of m traces and n samples per trace, the main steps of FX Cadzow filtering are as follows.

Step 1: Each trace of the input data is converted into the frequency domain by a Fourier transform. Assume that T is the transpose operator, and the result F is written as

$$F = [f_1 \ \cdots \ f_n]^T, f_i = [f_{i,1} \ \cdots \ f_{i,m}], \quad i = 1, \dots, n. \quad (1)$$

Step 2: Assume that $0 < q < m$. Each f_i is embedded in an associated Hankel matrix M_i written as

$$M_i = \begin{bmatrix} f_{i,1} & f_{i,2} & \cdots & f_{i,m-q+1} \\ f_{i,2} & f_{i,3} & \cdots & f_{i,m-q+2} \\ \vdots & \vdots & \ddots & \vdots \\ f_{i,q} & f_{i,q+1} & \cdots & f_{i,m} \end{bmatrix}. \quad (2)$$

Step 3: Assume H is the conjugate transpose operator. The SVD of each M_i is given as

$$M_i = \sum_{j=1}^n u_j \lambda_j v_j^H \quad (3)$$

where u_j and v_j denote the j th left singular vector and the j th right singular vector, respectively, and their corresponding singular value is λ_j and $\lambda_j \geq \lambda_{j+1}$. The low-rank approximation \tilde{M}_i with rank r is written as

$$\tilde{M}_i = \sum_{j=1}^r u_j \lambda_j v_j^H, r < n. \quad (4)$$

Step 4: Each \tilde{f}_i is recovered by the average values of the antidiagonal elements of its associated \tilde{M}_i . The filtered result \tilde{F} is expressed as

$$\tilde{F} = [\tilde{f}_1 \ \cdots \ \tilde{f}_n]^T. \quad (5)$$

Finally, the filtered result is obtained by converting each trace of \tilde{F} back to the time domain via an inverse Fourier transform.

B. Random-Derangement-Based FX Cadzow Filter

When reflections are overlapped or even overwhelmed by MRRs, the FX Cadzow filter removes some reflection components when filtering the MRRs. To better preserve reflection components and attenuate MRRs, the random-derangement-based FX Cadzow filter is designed for attenuating MRRs group by group.

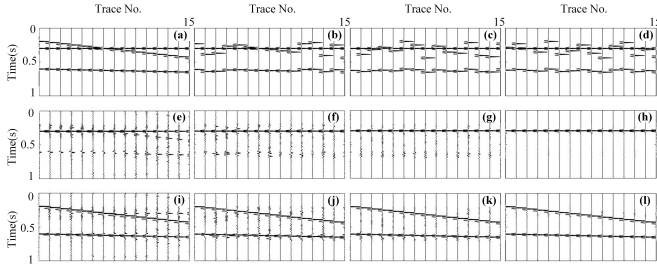


Fig. 2. Experiment results. (a) Synthetic data. (b) and (c) Two rearrangements after the general random operator. (d) Rearrangement after the random derangement operator. (e)–(h) Filtered data from (a)–(d) after filtering. (i)–(l) Differences between (e) and (a), (f) and (a), (g) and (a), and (h) and (a).

Since the data obtained by bilateral acquisition can be divided into two unilateral data for processing, the input common-shot gather \mathbf{Y} is assumed to be obtained by unilateral acquisition. To flatten a group of MRR events, different \mathbf{Y} matrices are covered by LMO with different dips starting from an initial dip. The $R_{\text{LMO}}^k(\mathbf{Y})$ is defined as one matrix after the LMO with dip k . Our purpose is to use the first several singular values to reconstruct a group of flattened MRRs. Among matrices after LMO with different dips, the matrix $R_{\text{LMO}}^k(\mathbf{Y})$ with the largest first singular value [5] is regarded as the contaminated region with flattened MRRs. In practice, consider the spatial variations during the seismic wave propagation, the contaminated region is divided into several small overlapping windows of the same size. These windows are randomized and filtered one by one. The size of each window should make local MRR events horizontal, but cannot be too small, or else the filtering performance will be poor.

Assume that $R_{\text{LMO}}^*(\mathbf{Y})$ consists of m traces in the spatial direction. The general random operator randomly rearranges trace orders of $R_{\text{LMO}}^*(\mathbf{Y})$ based on the Fisher–Yates algorithm [28] that generates $m!$ possible rearrangements for a randomization, where $!$ denotes the factorial operator. To obtain the rearrangements that lead to good filtering performance, a random derangement operator $R_r(\cdot)$ that randomly deranges trace orders $R_{\text{LMO}}^*(\mathbf{Y})$ based on a rejection method [29] is proposed. The rejection method quickly generates a new permutation by resampling orders from the input trace orders with uniform distribution. Trace orders in new permutation are not repeated. Assume that $F_c(\cdot)$ denotes the FX Cadzow filtering operator. The result $\tilde{\mathbf{Y}}$ from FX Cadzow filtering is written as

$$\tilde{\mathbf{Y}} = F_c(R_r(R_{\text{LMO}}^*(\mathbf{Y}))). \quad (6)$$

The filtered data \mathbf{Y}' from the proposed method are written as

$$\mathbf{Y}' = \mathbf{Y} - (R_{\text{LMO}}^*((R_r(\tilde{\mathbf{Y}}))^{-1}))^{-1} \quad (7)$$

where $R_r(\cdot)^{-1}$ denotes the inverse random derangement operator and $R_{\text{LMO}}^*(\cdot)^{-1}$ denotes the inverse LMO operator. We then return to the beginning with \mathbf{Y}' as input until all groups of MRRs are attenuated.

An experiment is used to demonstrate the influence of different rearrangements on filtering performance. The 2-D synthetic data with SNR of -2.00 dB are shown in Fig. 2(a). It consists of 15 traces and 1001 samples per trace and contains a horizontal event and two dipping events, one of

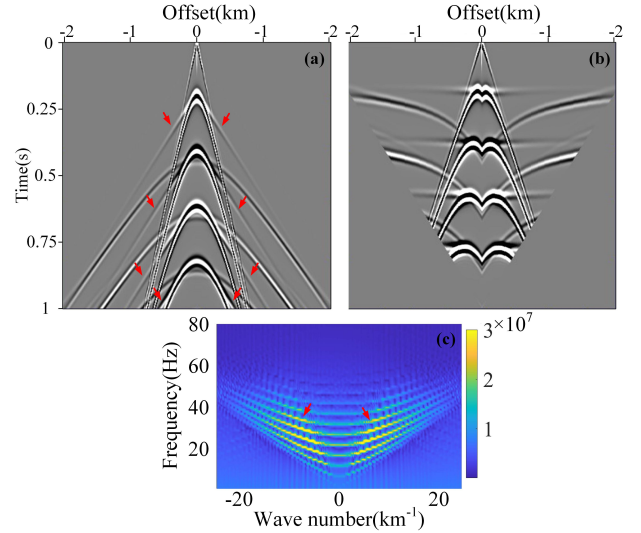


Fig. 3. 2-D synthetic data. (a) 2-D synthetic data. (b) Data after LMO. (c) FK spectrum of (a).

which is with a small dip close to zero. The window is with a spatial dimension of 15 traces and a time dimension of 1000 ms. The largest singular value is used to reconstruct. Two rearrangements after the general random operator are randomly selected and shown in Fig. 2(b) and (c), respectively. A randomly selected rearrangement after the random derangement operator is shown in Fig. 2(d). The data obtained by applying the FX Cadzow filter to Fig. 2(a)–(d) are shown in Fig. 2(e)–(h). Differences between Fig. 2(a) and (e), Fig. 2(a) and (f), Fig. 2(a) and (g), and Fig. 2(a) and (h) are shown in Fig. 2(i)–(l), respectively. Fig. 2(h) and (l) shows the purest horizontal event and dipping events, respectively. There are fewer residual dipping events in Fig. 2(g) than in Fig. 2(f). Fig. 2(e) shows the most residual dipping events. There is a less residual horizontal event in Fig. 2(k) than in Fig. 2(j). Fig. 2(i) shows the most residual horizontal event. The SNRs of Fig. 2(e)–(h) are 6.13, 7.63, 12.41, and 18.84 dB, respectively. Due to the limited spatial dimension of the window, the original data and two rearrangements after the general random operator lead to undesirable filtering performance. The rearrangement after random derangement operator still leads to good filtering performance.

III. DATA EXAMPLES

A. Synthetic Data Example

Our method and 2-D FK filters are tested on the 2-D synthetic data. As shown in Fig. 3(a), the synthetic data are modeled by the ground over a low-velocity layer with a thickness of 80 m. Below the low-velocity layer, there is a high-velocity layer with a thickness of 300 m. Their velocities are 800 and 2500 m/s, respectively. The density of each layer varies laterally, which is adaptively calculated by the Garden formula. The synthetic data obtained are based on the wave equation forward modeling with a Ricker of 30 Hz. The maximum offset is 2000 m, and the trace interval is 5 m. The total sampling time is 1 s, with a sampling interval of 0.001 s. There are a group of MRR events pointed by red arrows in Fig. 3(a). The data after LMO are shown in Fig. 3(b), and its

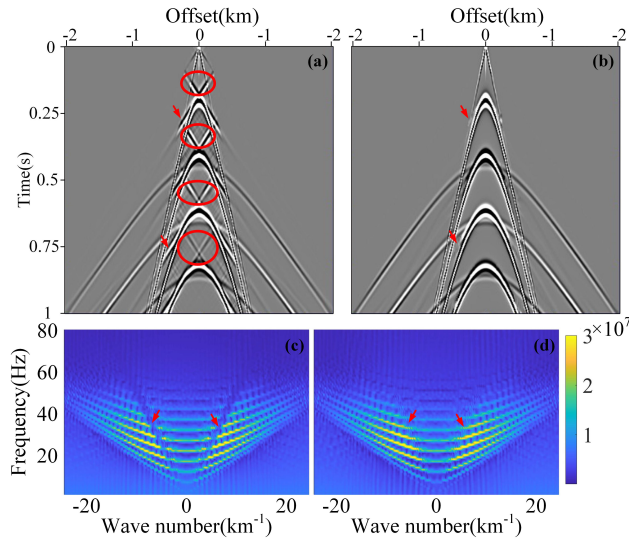


Fig. 4. Filtered data. (a) Filtered data after FK filtering. (b) Filtered data after the proposed method. (c) FK spectrum of (a). (d) FK spectrum of (b).

FK spectrum is shown in Fig. 3(c), where reflections and MRR overlap each other. The window is with a spatial dimension of 25 traces and a time dimension of 1000 ms. We maintain the largest singular value for reconstruction.

The filtered data after 2-D FK filtering are shown in Fig. 4(a), with its FK spectrum shown in Fig. 4(c). The filtered data after the proposed method are shown in Fig. 4(b), with its FK spectrum shown in Fig. 4(d). Fig. 5(a) and (b) shows the differences between Figs. 3(a) and 4(a) and Figs. 3(a) and 4(b). Fig. 5(c) and (d) shows the FK spectra of Fig. 5(a) and (b). Fig. 3(b) shows that the MRR events are relatively horizontal after LMO. Less MRRs are shown in Fig. 4(a) and (b) than in Fig. 3(a). But take the regions indicated by arrows as examples, Fig. 4(a) shows obvious residual MRRs while no visible residual MRRs are shown at the same positions in Fig. 4(b). Some artifacts are circled by some red ellipses in Fig. 4(a). The same positions in Fig. 4(b) are clear. Such findings illustrate that 2-D FK filter oversmears the amplitude of the input data. In addition, take the regions indicated by arrows in Figs. 4(c), (d), and 3(c) as examples, the reflection energy is more consistent in Fig. 4(c) than in Fig. 4(d). No visible reflections are shown in Fig. 5(b). But reflections in Fig. 5(a) are obvious.

B. Field Data Example

Then, our method and 2-D FK filter are applied to the 2-D common-shot gather shown in Fig. 1. It is obtained by bilateral acquisition and consists of 255 traces with 3501 samples per trace. The trace interval is 20 m and the sampling interval is 0.001 s. Its FK spectrum is shown in Fig. 7(a) where the reflection energy is overwhelmed by the MRR energy, and this is indicated by red arrows in the regions. The window is with a spatial dimension of 15 traces and a time dimension of 3500 ms. We maintain the largest singular value for reconstruction. There are some regions in these data contaminated with the ground roll, but the implicated locating method will avoid them.

Fig. 6(a) and (b) shows the filtered data after 2-D FK filtering and our method, respectively. The differences

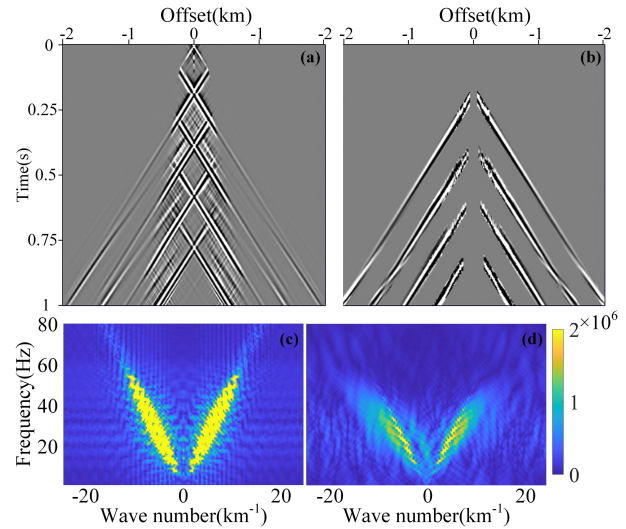


Fig. 5. Differences. (a) Difference between Fig. 2(a) and 3(a). (b) Difference between Fig. 2(a) and (b). (c) FK spectrum of (a). (d) FK spectrum of (b).

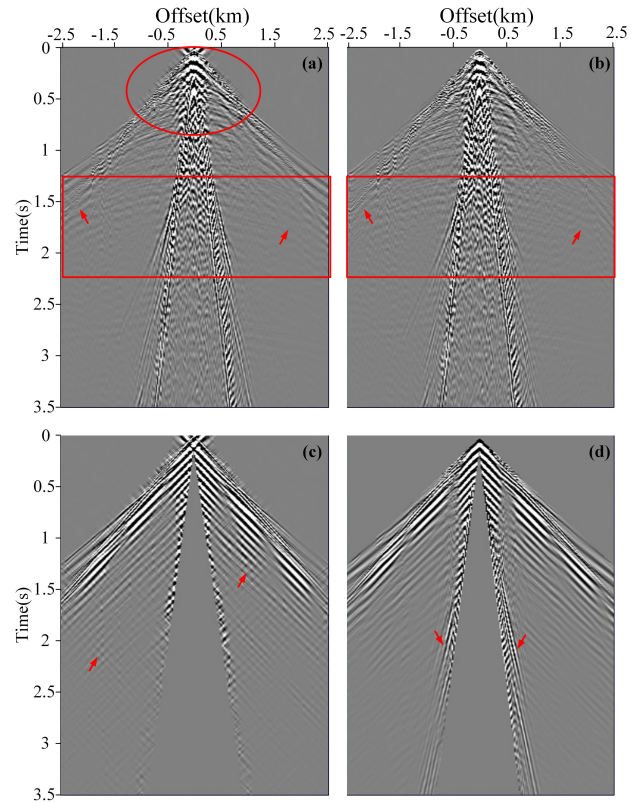


Fig. 6. Results. (a) Filtered data after 2-D FK filtering. (b) Filtered data after the proposed method. (c) Difference between Fig. 1 and (a). (d) Difference between Fig. 1 and (b).

between Figs. 1 and 6(a) and Figs. 1 and 6(b) are shown in Fig. 6(c) and (d). The reflection events are clearer in Fig. 6(c) and (d) than in Fig. 1. Take the regions in the red rectangles in Fig. 6(a) and (b) as examples, reflection events are clear in Fig. 6(b), but overwhelmed by the obvious MRRs indicated by red arrows in Fig. 6(a). As shown in Fig. 6(c) and (d), especially between 2.5 and 3.5 s, the MRR energy in Fig. 6(d) is more consistent than in Fig. 6(c). Parts of the linear ground roll, such as those indicated by red arrows in Fig. 6(d), are also removed. Artifacts exist in the red

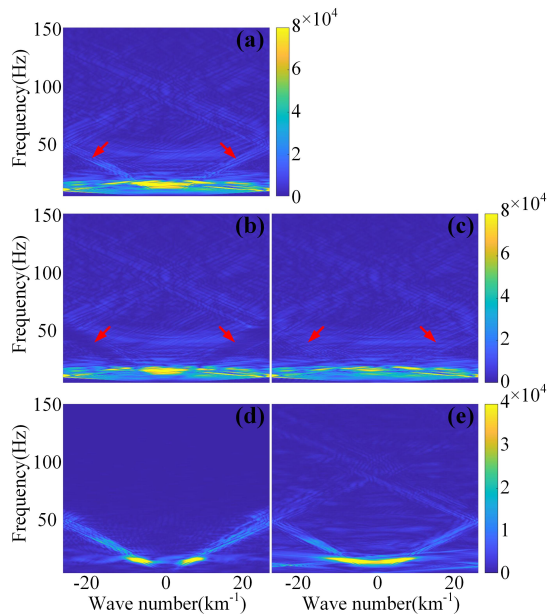


Fig. 7. FK spectra. (a) FK spectrum of Fig. 1. (b) FK spectrum of Fig. 6(a). (c) FK spectrum of Fig. 6(b). (d) FK spectrum of Fig. 6(c). (e) FK spectrum of Fig. 6(d).

ellipse in Fig. 6(a) and those regions indicated by red arrows in Fig. 6(c), but not in the same positions in Fig. 6(b) and (d).

The FK spectra of Fig. 6(a) and (c) are shown in Fig. 7(b) and (c). Fig. 7(d) and (e) shows the FK spectra of Fig. 6(c) and (d), respectively. Take the regions indicated by the red arrows as examples, the reflection energy is more consistent in Fig. 7(b) than in Fig. 7(c). In other words, the 2-D FK filter separates the reflection energy in its stopband when suppressing MRRs. Take the regions near the red arrows as examples, the reflection energy is more apparent in Fig. 7(c) than in Fig. 7(a). More aliased MRR energy is shown in Fig. 7(e) than in Fig. 7(d), indicating that our method can also handle the spatially aliased data.

IV. CONCLUSION

In this letter, a random-derangement-based FX Cadzow filter is proposed, which attenuates MRRs in a 2-D common-shot gather. Our filter is designed based on the linear events of MRRs and the randomization of limited trace orders of the input data. A random derangement operator is incorporated into this filter, which is based on a rejection method to obtain a rearrangement after randomization that leads to better filtering performance. Both 2-D synthetic data and 2-D field data demonstrate that our filter outperforms the 2-D FK filter in attenuating both aliased and nonaliased MRRs. Our filter preserves reflections better without creating artifacts and can be extended to multiple dimensions beyond 2-D and possibly used to attenuate linear ground roll. The way of obtaining desirable rearrangement after a randomization can be improved further in our next work.

REFERENCES

- [1] C. P. Ross, "AVO in the presence of coherent noise," *Lead. Edge*, vol. 12, no. 3, pp. 196–201, Mar. 1993.
- [2] W. Huang, R. Wang, Y. Zhou, and X. Chen, "Simultaneous coherent and random noise attenuation by morphological filtering with dual-directional structuring element," *IEEE Geosci. Remote Sens. Lett.*, vol. 14, no. 10, pp. 1720–1724, Oct. 2017.

- [3] W. Chen, J. Xie, S. Zu, S. Gan, and Y. Chen, "Multiple-reflection noise attenuation using adaptive randomized-order empirical mode decomposition," *IEEE Geosci. Remote Sens. Lett.*, vol. 14, no. 1, pp. 18–22, Jan. 2017.
- [4] P. G. Kelamis and D. J. Verschuur, "Surface-related multiple elimination on land seismic data—Strategies via case studies," *Geophysics*, vol. 65, no. 3, pp. 719–734, May 2000.
- [5] R. Montagne and G. L. Vasconcelos, "Optimized suppression of coherent noise from seismic data using the Karhunen-Loève transform," *Phys. Rev. E, Stat. Phys. Plasmas Fluids Relat. Interdiscip. Top.*, vol. 74, no. 1, Jul. 2006, Art. no. 016213.
- [6] H. Changqing, F. Dehua, L. Zhenkua, W. Jianmin, and F. Zhaokui, "Shallow multiple refraction mechanism and application in seismic acquisition," in *Proc. SPG/SEG Beijing Int. Geophys. Conf.*, Apr. 2016, pp. 318–321.
- [7] M. Gadallah and R. Fisher, "Seismic data processing," in *Exploration Geophysics*. Berlin, Germany: Springer, 2009, vol. 22, pp. 85–95.
- [8] W. Wang, S. Hao, H. Liu, and Z. Sun, "High resolution τ -p transform in linear events wavefield separation," *Prog. Geophys.*, vol. 21, no. 1, pp. 74–78, 2006.
- [9] J. Fan, Z. Li, X. Song, K. Zhang, and Q. He, "Application of anisotropic high-resolution Radon transform for multiple attenuation," *SEG Tech. Program Expanded Abstr.*, pp. 4580–4584, 2015.
- [10] F. J. Herrmann, D. Wang, and D. J. Verschuur, "Adaptive curvelet-domain primary-multiple separation," *Geophysics*, vol. 73, no. 3, pp. 17–21, 2008.
- [11] L. J. A. D. Almeida, R. R. Manenti, and M. J. Porsani, "Coherent noise attenuation using the wavelet transform on radial basis," *Revista Brasileira de Geofísica*, vol. 34, no. 4, pp. 4720–4724, Jun. 2017.
- [12] S. K. Chiu and J. E. Howel, "Attenuation of coherent noise using localized-adaptive eigenimage filter," *SEG Tech. Program Expanded Abstr.*, pp. 2541–2545, 2008.
- [13] W. J. Done, R. L. Kirlin, and A. Moghaddamjoo, "Two-dimensional coherent noise suppression in seismic data using eigendecomposition," *IEEE Trans. Geosci. Remote Sens.*, vol. 29, no. 3, pp. 379–384, May 1991.
- [14] S. L. M. Freire and T. J. Ulrych, "Application of singular value decomposition to vertical seismic profiling," *Geophysics*, vol. 53, no. 6, pp. 778–785, Jun. 1988.
- [15] X. Liu, "Ground roll suppression using the Karhunen-Loeve transform," *Geophysics*, vol. 64, no. 2, pp. 564–566, Mar. 1999.
- [16] S. Trickett, "Eigenimage noise suppression of 3D seismic in the FXY domain," *SEG Tech. Program Expanded Abstr.*, pp. 1981–1984, 2001.
- [17] S. Trickett and L. Burroughs, "Prestack rank-reduction-based noise suppression," *Recorder*, vol. 34, no. 9, pp. 3193–3196, 2009.
- [18] S. Trickett, "F-xy Cadzow noise suppression," *SEG Tech. Program Expanded Abstr.*, pp. 2586–2590, 2008.
- [19] A. C. C. Mançur, "Iterative SSA method to filtering of the land seismic data," *SEG Global Meeting Abstr.*, pp. 1528–1531, 2017.
- [20] V. Oropeza and M. Sacchi, "Multifrequency singular spectrum analysis," *SEG Tech. Program Expanded Abstr.*, pp. 3193–3197, 2009.
- [21] J. Cadzow, "Effective reflection enhancement a composite property mapping algorithm," *IEEE Trans. Acoust., Speech Effective Reflection Process.*, vol. 36, pp. 1–62, 1988.
- [22] V. Oropeza and M. Sacchi, "Application of singular spectrum analysis to ground roll attenuation," *GeoCanada, Tech. Rep.*, 2010.
- [23] V. Oropeza and M. Sacchi, "Simultaneous seismic data denoising and reconstruction via multichannel singular spectrum analysis," *Geophysics*, vol. 76, no. 3, pp. 25–32, 2011.
- [24] S. K. Chiu, "Coherent and random noise attenuation via multichannel singular spectrum analysis in the randomized domain," *Geophys. Prospecting*, vol. 61, pp. 1–9, Jun. 2013.
- [25] W. Huang *et al.*, "Randomized-order multichannel singular spectrum analysis for simultaneously attenuating random and coherent noise," *SEG Tech. Program Expanded Abstr.*, pp. 4777–4781, 2016.
- [26] J. Ma, "Random low patch-rank method for interpolation of regularly missing traces," *J. Harbin Inst. Technol.*, vol. 27, pp. 205–216, 2020.
- [27] H. Lindi, F. Bayati, and H. Siahkoohi, "Attenuating GR by using SVD in F-X domain after applying LMO," in *Proc. Int. Geophys. Conf. Oil*, 2013, pp. 1–4.
- [28] D. Richard, "Algorithm 235: Random permutation," *Commun. ACM*, vol. 7, no. 7, pp. 517–534, 1964.
- [29] C. Martínez, A. Panholzer, and H. Prodinger, "Generating random derangements," in *Proc. 5th Workshop Analytic Algorithmics Combinatorics (ANALCO)*, Jan. 2008, pp. 234–240.